Decoding temporal interpretation of the morphogen Bicoid in the early *Drosophila* embryo

Anqi Huang[1*], Christopher Amourda[1*], Shaobo Zhang[1], Nicholas S. Tolwinski[2,3], and Timothy E. Saunders[1,3,4]

[1]Mechanobiology Institute, National University of Singapore, T-Lab, 5A Engineering Drive 1, Singapore 117411
[2]Division of Science, Yale-NUS College, 12 College Ave West, #01-201, Singapore 138610
[3]Department of Biological Sciences, National University of Singapore, 14 Science Drive 4, Singapore 117543
[4]Institute for Molecular and Cell Biology, Agency for Science Technology and Research, 61 Biopolis Dr, Singapore 138673
* These authors contributed equally
Correspondence: dbsste@nus.edu.sg

SUMMARY

Morphogen gradients provide essential spatial information during development. Not only the local concentration but also duration of morphogen exposure is critical for correct cell fate decisions. Yet, how and when cells temporally integrate signals from a morphogen remains unclear. Here, we use optogenetic manipulation to switch off Bicoid-dependent transcription in the early *Drosophila* embryo with high temporal resolution, allowing time-specific and reversible manipulation of morphogen signalling. We find that Bicoid transcriptional activity is dispensable for embryonic viability in the first hour after fertilization, but persistently required throughout the rest of the blastoderm stage. Short interruptions of Bicoid activity alter the most anterior cell fate decisions, while prolonged inactivation expands patterning defects from anterior to posterior. Such anterior susceptibility correlates with high reliance of anterior gap gene expression on Bicoid. Therefore, cell fates exposed to higher Bicoid concentration require input for longer duration, demonstrating a previously unknown aspect of morphogen decoding.

INTRODUCTION

Morphogens are molecules distributed in spatial gradients that provide essential positional information in the process of development (Turing, 1990; Wolpert, 1969). By activating differential gene expression in a concentration-dependent manner, morphogens instruct the cells to adopt proper cell fates according to their positions in the developing embryos or tissues (Gurdon and Bourillot, 2001; Neumann and Cohen, 1997). The impact of a morphogen gradient on a developing system depends on two characteristics: first, its information capacity in terms of how many distinct cell types it has an effect on; second, its transferring precision – in essence, how reproducible cell fates are in different individuals at given positions. Each of these characteristics depends not only on the local concentration of morphogen molecules that the cells interpret, but also temporal components of such interpretation.

The temporal pattern of morphogen interpretation has been demonstrated in several vertebrate developing systems. Harfe et al. first proposed that the length of time of morphogen signalling is critical for correct cell fate specification. They found that during mouse limb development, cells exposed to Sonic Hedgehog (Shh) morphogen for longer time develop into digits of more posterior identity (Harfe et al., 2004). Similarly, in chick neural tube formation the duration of Shh activity is translated into different cell types along the dorso-ventral axis (Dessaud et al., 2007). In comparison, in fish dorso-ventral patterning it is not the duration but the timing of BMP signaling that is important for correct cell fate determination (Tucker et al., 2008). While in some cases the temporal integration of morphogen signaling is carried out by genetic feedback loops (Dessaud et al., 2010), in many other systems the underlying mechanism has not been unveiled.

As the first protein identified to function as a morphogen, Bicoid (Bcd) patterns the cells along the antero-posterior axis in the early embryo of the fruitfly, *Drosophila melanogaster* (Driever et al., 1989). Bcd is maternally deposited and localized at the anterior pole of the embryo in the form of mRNA (Frohnhöfer and Nüsslein-Volhard, 1986). This localized mRNA is further translated upon fertilization, forming a protein gradient with exponential decay in concentration along the antero-posterior axis. Fundamentally acting as a transcription factor, Bcd activates different genes, with the more anteriorly expressed genes having lower Bcd binding affinity (Struhl et al., 1989). Quantitative studies have shown that the Bcd gradient is highly dynamic, with nuclear Bcd concentration constantly changing throughout the first 13 rounds of syncytial cell divisions (Little et al., 2011). It has been suggested that precise positional information endowed by Bcd gradient at one single time point suffices to distinguish neighbor cell identities (Gregor et al., 2007a). However, recent results have motivated intense debate over what is the exact time window when the information carried by Bcd is interpreted (Bergmann et al., 2007; Gregor et al., 2007b; Liu et al., 2013; Lucchetta et al., 2005).

To address this question, fast and reversible temporal manipulation of Bcd activity is required. In this study, we have developed an optogenetic tool to control Bcd-dependent transcription in the early *Drosophila* embryo with high temporal resolution. Using this tool, we provide a detailed dissection of the temporal components of Bcd decoding *in vivo*. The results unveil an unexpected temporal pattern of Bcd action – cell fates determined by higher Bcd concentration require Bcd for longer duration, while cells experiencing lower Bcd dosage commit to correct fates at earlier developmental stages. Further combining temporal perturbation with quantitative analyses, we find that the differential expression kinetics of target genes can partly explain the mechanism underlying such temporal interpretation.

RESULTS

Precise temporal control of Bcd-dependent transcription via optogenetic manipulation

We built a light-responsive construct to switch off Bcd-dependent transcription by fusing the optogenetic cassette cryptochrome 2 (CRY2) together with mCherry (mCh) to the N-terminus of Bcd (Kennedy et al., 2010) (Figure 1A). We used standard P-element transformation to insert this CRY2::mCh::Bcd construct at different genomic loci generating diverse fly lines expressing this fusion protein at various levels under the control of the endogenous bcd regulatory sequences.

We find that in the dark, CRY2::mCh::Bcd transgenics rescues the absence of endogenous Bcd. The expression patterns of four gap genes – *hunchback* (*hb*), *giant* (*gt*), *krüppel* (*kr*) and *knirps* (*kni*) – are reminiscent of wild-type embryos when the light-responsive Bcd construct is expressed in an otherwise *bcd* mutant background (Figures 1B-1E). These embryos hatched as healthy larvae (Figure 1F). In comparison, embryos illuminated with blue light during the first 2.5 hours after egg deposition show severe defects in the anterior, Bcd-dependent, expression domains of *hb*, *gt* and *kni*, while their posterior counterparts remain intact (Figures 1G, 1H, and 1I). Furthermore, the Kr band shifts anteriorly when compared to the pattern observed in the dark (Figures 1E and 1J, arrowheads). Illuminated embryos fail to develop the head and thorax structures (Figure 1K), resembling the *bcd* knockout phenotype (Figure 1L). Altogether, these data indicate that the blue light-induced conformational change of CRY2 inhibits Bcd-dependent gene expression. We quantified the Bcd gradient under dark and illuminated conditions (Figures 1M and 1N) and observed no significant change in Bcd profile (Figure 1O), showing that the spatial distribution of Bcd molecules is not affected by our manipulation. Besides acting as a transcription factor, Bcd also represses translation of Caudal (Cad) mRNA at the anterior region of the embryo. Remarkably, we saw no shift in

Cad gradient in illuminated embryos when compared to those in the dark (Figures 1P-1R), suggesting that light-induced conformational changes did not alter the translation inhibitory capability of Bcd in the cytoplasm. This allows us to dissociate transcriptional and translational roles of Bcd.

Next we tested whether CRY2::mCh::Bcd under illumination inhibits transcription in a dominant negative manner. We selected two fly lines expressing CRY2::mCh::Bcd at comparatively lower and higher levels in a *bcd* wild-type background, denoted by $CRY2^{low}$ and $CRY2^{high}$, respectively (Figures S1A and 1B) and utilized the MS2 system to visualize the transcriptional activity of the Bcd target gene *hb* (Garcia et al., 2013; Lucas et al., 2013). Compared to wild-type embryos - where transcriptional activity of *hb* in the Bcd-dependent anterior domain persists throughout the interphase of nuclear cycle (n.c.) 13 (7.1 ± 3.2 min; Figures 2A and 2B, Movie S1) - $CRY2^{low}$ embryos show significantly reduced transcriptional persistence when illuminated with a 488 nm laser (3.6 ± 1.1 min; Fig.2a, c). Such an inhibitory effect becomes more prominent in $CRY2^{high}$ embryos (3.0 ± 0.5 min, Figures 2A and 2D). The transcription of the posterior *hb* domain is Bcd-independent and, reassuringly, we do not observe any inhibitory effect in this domain (4.3 ± 2.0 min, 5.2 ± 3.3 min, and 4.2 ± 2.0 min in control, $CRY2^{low}$, and $CRY2^{high}$, respectively; Figure 2E). Further, the inhibitory effect for the same genetic background and illumination conditions is uniform along the AP axis (Figures S1C and S1D). As parallel evidence, ChIP-qPCR experiments show comparable CRY2::mCh::Bcd binding in dark or light to native Bcd binding sites (Figure 2F), with no noticeable unspecific DNA binding caused by light-induced conformational changes (Figure 2G).

We then explored the effect of tuning the inhibition of Bcd-dependent transcription by varying the blue-light illumination intensity. We illuminated embryos with blue light at

different powers (0.04, 0.4 and 4 mW) during the hour prior to gastrulation. We used the Even-skipped (Eve) pattern, where Eve stripes 1 and 2 are Bcd-dependent and more posterior stripes are Bcd-independent as a readout of Bcd activity (Frasch and Levine, 1987; Stanojevic et al., 2016). In a WT background, low power illumination (0.04 mW) causes a moderate reduction and a slight anterior shift of the Eve stripes 1 and 2 expression (Figures 2H and 2I). Increasing light power further decreases the expression level of the first two Eve stripes (Figures 2J and 2K). When expressed in a *bcd* null background, CRY2::mCh::Bcd completely inhibits the expression of the anterior two Eve stripes, even at the lowest light power tested (Figures 2L and 2O).

Putting the above results together, blue light illumination induces a light-sensitive conformational change of the N-terminal CRY2, resulting in the inhibition of Bcd-dependent target gene transcription by, potentially, hindering the assembly of the transcription machinery. CRY2::mCh::Bcd under illumination competes with wild-type Bcd protein for binding to the native Bcd DNA binding sites, therefore acting as a dominant negative transcription factor. This inhibitory effect was stronger in a *bcd* null background, likely due to the lack of competitive binding. These effects were reversible upon returning to a dark state (see results below and references Guglielmi et al., 2015; Kennedy et al., 2010). Finally, the light-induced conformational change does not affect Bcd's role in translational repression of Cad mRNA. This may be one of the reasons that gap gene expression in illuminated embryos does not perfectly recapitulate that in *bcd* null embryos, where both Bcd transcriptional and translational effects are lost (Figure S2).

Persistent Bcd transcription activity is indispensable to embryonic viability

Bcd confers robust cell fate decisions by activating hierarchical segmentation gene networks (Jaeger et al., 2004; Kraut and Levine, 1991; Manu et al., 2009). Previous studies have shown that only at early n.c. 14 is the absolute Bcd concentration interpreted as positional information. In late n.c. 14, on the contrary, expression boundaries of downstream genes are subjected to cross-regulation and the Bcd gradient is believed to no longer be important (Liu et al., 2013). To determine whether Bcd-dependent transcription in late n.c. 14 is actually irrelevant for cell fate determination, we collected embryos laid by females expressing CRY2::mCh::Bcd in a *bcd* null background ($CRY2^{high}$, bcd^{-}; in all following experiments unless otherwise stated) and illuminated them before the initiation of gastrulation for time windows ranging from 10 to 60 minutes (Figure 3A). Surprisingly, 10 minutes of illumination at the end of n.c. 14 is sufficient to induce embryonic lethality. Cuticle preparation of these non-hatched embryos shows defective mouthparts, in particular the pharynx (Figures 3B and 3C, arrows). In addition, the structures between mouth hooks and cephalo-pharyngeal plates are missing (Figure 3C, arrowhead). Thirty minutes of illumination causes further deterioration in mouth development, with minimal mouth skeleton visible (Figure 3D). Extending the illumination window depletes all mouthparts (Figures 3E and 3F), with the most severe phenotypes observed when illumination encompasses both n.c. 13 and n.c. 14. Under this condition, all thorax segments are lost, with only abdominal denticle belts remaining (Figure 3F).

Transcripts of Bcd target genes have been detected using *in situ* hybridization at time points as early as n.c. 7 (Ali-Murthy and Kornberg, 2016). We tested whether such early Bcd-dependent transcription was essential for embryonic viability by illuminating embryos during early developmental stages (*i.e.* before n.c. 14) and reverting them later to dark conditions to

recover Bcd-dependent transcription. We find that a 30-minute illumination window spanning n.c. 11~13 results in severe patterning defects (Figure 3G), phenocopying the embryos illuminated during n.c. 13 and 14 (Figure 3F). This suggests that Bcd-dependent transcription before n.c. 14 is indispensable for initiating its downstream gene cascade. Shifting the 30-minute illumination period to 10 minutes earlier results in the recovery of proper thoracic segment patterning (Figure 3H, arrowhead). As the illumination time window is shifted sequentially earlier, more thorax and mouthparts are successively recovered (Figures 3I-3K). Last, when the illumination time window is shifted before n.c. 10 (Figure 3K), the cuticle patterns become equivalent to those of embryos developed in the dark (Figure 3B) and, moreover, the larval hatchability reaches that of dark conditions.

These temporal perturbation experiments reveal that persistent Bcd-dependent transcription activity from n.c.10 is required for robust embryonic patterning, and ultimately embryonic viability. In contrast, formation of the more posterior, thoracic segments is only perturbed when extended illumination covers n.c.13, the critical time window for properly initiating the downstream gene cascade.

Anterior cell fates require Bcd-dependent transcription for longer duration

Deprivation of Bcd-dependent transcription in late blastoderm stages leads to embryonic lethality, due to errors in cell fate determination. To determine which cell fates are altered by the lack of Bcd function (Figure 4A), we fixed illuminated CRY2^{high}, *bcd*$^{-}$ embryos at the end of germband extension (GBE, 4 hours after gastrulation initiates) and analyzed the expression of Engrailed (En) and various Hox genes. The most anterior morphological features that can be observed at GBE are the clypeolabrum lobe at the very tip of the embryo and the invagination of stomodeum (Figure 4B, red and orange dots, respectively). Blue-light

illumination for 10 minutes before gastrulation impairs the formation of these very anterior structures while the expression of the more posterior En stripes remains intact (Figure 4C). Extending illumination to 30 minutes prior to gastrulation, we observe the loss of the next two En stripes marking the mandibular (Mn) and maxillary (Mx) segments (Figure 4D). Concomitantly, we observe diminished expression of Deformed, a Hox gene that controls morphogenesis of these same Mn and Mx segments (Figure 4D'). This suggests that presumptive Mn and Mx cells commit to alternative cell fates. Similarly, 50 minutes of illumination prior to gastrulation results in the loss of expression of Sex Comb Reduced (Scr), the hox gene that regulates development of the labial segment (Figures 4E' and 4E''). This correlates with the loss of the En stripe marking this very same segment (Figure 4E). Further extending illumination, we observe that anterior cells adopt posterior cell fates, reflected in the ectopic expression of Ultrabithorax (Ubx) and Abdomen-B (Abd-B) in anterior regions (Figures 4E'', 4F'' and S3F'', arrows). In the most severe case, we see that all En segments from the anterior to the third thorax (T3) are missing (Figure 4F).

Sequential disappearance of En stripes from anterior to posterior correlates with prolonged illumination at the end of the blastoderm stage. This evidence shows that more anterior cell fates require Bcd-dependent transcription to persist until the very end of n.c. 14. In contrast, cells in more posterior regions undergo correct fate decisions at earlier stages, regardless of the Bcd transcription activity at later time points.

Temporal dissection of Bcd target gene expression

To gain deeper insight into the molecular basis of the spatio-temporal readout dependence on Bcd, we investigated how deprivation of Bcd-dependent transcription at different time windows affects downstream gap gene expression. To this end, we inhibited Bcd-dependent

transcription at precise time windows (Figure 5A), then fixed these embryos at the end of the blastoderm stage, and stained them for a range of gap genes.

First, we looked at the gap gene *hb*. Our live imaging (Figures 2A-2E) reveals that illumination significantly reduces the transcription activity of the *hb* anterior domain. Surprisingly, illumination during the last 30 minutes of the blastoderm stage does not affect Hb in neither protein level nor boundary position (Figure 5B), indicating that Hb expression is independent of the newly synthesized mRNA in the last 30 minutes of n.c. 14. This shows that the Hb protein level remains stable once the *hb* mRNA amount has exceeded a certain threshold value. However, extending illumination throughout n.c. 14 (or even earlier) results in deviations of the Hb anterior pattern (Figures 5B, arrows; and S4B4). It has previously been reported that the Hb pattern due to the activity of the *hb* stripe enhancer at the posterior border evolves during n.c. 14 from a shallow and broad gradient to a steep and sharp one (Perry et al., 2011, 2012). Here, we show that the mRNA synthesized prior to n.c. 14 is sufficient to support the formation of the broad gradient, as demonstrated by the Hb expression profile in embryos illuminated throughout cycle 14 (Figure 5B, curve 4). Transcriptional activity in the first 15 minutes of n.c. 14 is hence critical for precise formation of the wild-type Hb expression profile, at both anterior and posterior (driven by the stripe enhancer) borders. Further, continuous illumination throughout n.c. 13 and n.c. 14 severely impairs the anterior Hb expression level (Figures 5C and S4B5), showing that mRNA synthesized during n.c. 13 contributes significantly to the final Hb pattern. Interestingly, recovering the transcriptional activity during the last 30 minutes of n.c. 14 by reverting the embryos to the dark, results in a partial rescue of Hb anterior expression (Figure 5C, arrow), supporting the presence of a *hb* mRNA threshold. Nevertheless, transcription activity in late n.c. 14 fails to recover the stripe enhancer activity (Figure 5C, curve 1 and 6),

potentially due to shifted borders of posterior repressive factors. Next, we tested the contribution of *hb* transcription prior to n.c.13. Illumination during n.c. 10-12 results in a steep but narrow Hb gradient, where the posterior boundary shifts anteriorly by ~10% EL (Figure 5D). Illumination carried out before n.c. 11 results in a recovery of the shape of the Hb gradient when comparing to that of dark conditions, although the posterior border is still anteriorly shifted by 5% EL (Figures 5D, curve 8 and 5E-F, anterior shift indicated by red dashed line). This suggests that the production of zygotic *hb* transcription during n.c. 10-12 plays a critical role in *hb* auto-regulation, affecting the boundary positions of the mature Hb pattern. Therefore, we can temporally dissect Bcd-dependent activation of Hb, including separating the contributions from different enhancers.

The expression of the gap genes Kr (58-45% EL) and Kni (45-37% EL) is subjected to fine-tuning by Bcd-dependent transcription (in combination with Hb) (Hoch et al., 1991; Hülskamp et al., 1990). We find that the anterior boundary of Kr shows very high sensitivity to Bcd transcriptional inhibition - 20 minutes of illumination during the end of n.c. 14 causes an anterior shift by 3% EL, slightly widening the Kr domain (Figure 5G, 2, blue dot). Both the anterior and posterior borders of the Kr expression domain shift anteriorly upon illumination conditions 4, 5 and 6 (Figure 5G), correlating with the shift of the Hb boundary (Figures 5B curve 4 and 5C, curves 5 and 6). The strongest anterior shift of Kr boundaries is observed when embryos are reverted to dark after early illumination (Figure 5G, curve 6 and 7), as repressive Hb expression is anteriorly shifted (Figures 5C, curve 6 and 5D, curve 7) while Bcd transcriptional activity is recovered. The Kni anterior boundary shifts in correspondence with the posterior Kr boundary shifts, while its posterior boundary is much less sensitive (Figure 5H). In summary we find that the more anterior expression boundaries are located, the more susceptible they are to temporal inhibition of Bcd-dependent

transcription. Further, we find that a tight temporal interplay between Bcd and Hb is required for the precise positioning of gap gene expression boundaries.

Spatio-temporal atlas of Bcd decoding

We now construct a novel spatio-temporal atlas of Bcd-dependent gene transcription in the early *Drosophila* embryo, with clear time windows for gene activation (Figure 6A). A minimal 20-minute illumination at the end of n.c. 14 abolishes the expression of the Knirps anterior domain (Kni1) capping the tip of the embryo (Figures 6B and 6B'), as well as the first Giant stripe (Gt1) (Figures 6C and 6C'). Extending the Bcd inactivation across n.c. 14 further inhibits the gap gene expression domains located slightly more posterior, Orthodenticle (Otd) and the second Gt stripe (Gt2) (Figures 6C'', 6D and 6D'). Recovery of transcription activity in late stages fails to rescue the expression of most of these anterior gap gene domains (Figures S4C6, S4D6 and S4F6). When Bcd-dependent transcription is inhibited during n.c. 10-12 and then embryos returned to dark from n.c. 13, the time window for transcriptional recovery (approximately 1 hour) is insufficient to rescue the expression patterns of Kni1, Gt1 and Otd (Figures S4C7, S4D7, S4F7). This supports a mechanism whereby Bcd-dependent transcription serves a priming role prior to n.c. 13 to activate anterior segmentation genes at later stages. Such a priming role is stage-specific, as it is not compensated by late recovery of Bcd transcriptional activity. In comparison, illumination for 30 minutes before n.c. 10 has no apparent impact on segmentation gene expression (Figures S4B8-S4G8), corroborating previous results (Figure 3) indicating that Bcd-dependent transcription in this time window is dispensable for embryonic viability.

The reliance of the most anterior gap gene expression (Kni1, Gt1, and Otd) on persistent Bcd-dependent transcription may explain our previous observations that inhibiting Bcd

transcriptional activity both at very late or early stages impairs the proper formation of the anterior-most segments (Figures 3C, 3J and 4C). Any short interruption of Bcd transcriptional activity (from n.c. 10 till the very end of n.c. 14) abolishes the activation or maintenance of gap gene expression domains. As they lie on top of the hierarchical gene network defining cell fates, their loss alters cell fate decisions and leads to morphological defects. Comparatively, the expression of gap gene domains at posterior positions is less susceptible to perturbations in Bcd function. Consequently, cells arising from these domains still commit to correct fates under Bcd deprivation at early or late stages, as reflected in Hox gene expression patterns. We summarize this spatio-temporally coordinated Bcd interpretation in Figure 6E. The more anterior structures, which have cell fates governed by high Bcd concentration, require Bcd for an extended period of time. On the contrary, cells at positions responding to low Bcd require a markedly shorter time window of exposure to Bcd activity to commit to cell fates appropriate for their spatial position.

Discussion

Optogenetic manipulation of transcription activity *in vivo*

Several recent studies have used elegantly designed optogenetic systems to unveil the temporal role of signalling pathways in embryonic cell fate induction (Johnson et al., 2017; Sako et al., 2016). As a common strategy, an ubiquitously expressed construct is utilized to activate the upstream components of the signalling pathway in a light-responsive manner. In this study, we developed and characterized an optogenetic tool to temporally switch on and off of the transcriptional activity of the morphogen protein Bcd. In contrast to the previous approaches, our light-sensitive protein CRY2::mCh::Bcd is present in the spatial distribution of a native Bcd gradient. While the protein remains transcriptionally active in the dark, blue-light induced conformational change of N-terminal CRY2 abolishes all direct target gene expressions instantaneously. As such conformational change does not affect the DNA binding specificities (Figures 2F-2G) or the spatial localization of the protein (Figure 1O), we conclude that the inhibitory effect results from failure of transcriptional machinery assembly due to conformational hindrance. It remains unclear whether such hindrance is caused by the CRY2 conformational change alone or the effects of light-induced CRY2 oligomerization. It will be of general interest to further explore if the N-terminal CRY2 exerts transcriptional inhibition when tagged with other transcription factors, so that our optogenetic approach can be more widely applied to understand the temporal readout of spatially distributed transcription factors.

The temporal pattern of Bcd signal integration is spatially inhomogeneous

The continuous transitions between cell states in a developing embryo are governed by both the transcriptional landscape and the transcriptional history of the cells. Therefore, not only the local concentrations of the combinatorial transcription factors but also the timing and

duration of their presence are essential for the correct cell fate decisions. Bcd in the early fruit fly embryo provides the very initial positional cues along the antero-posterior axis, differentiating cells spanning ~10 embryonic segments (Driever et al., 1989). The gradient profile of Bcd is highly dynamic throughout the blastoderm stage, with no clear steady-state (Little et al., 2011). Such dynamics make the temporal aspects of Bcd interpretation critical for precise decoding of the morphogen. A previous study quantified the temporal evolution of Bcd dosage at several gap gene expression boundaries, and deduced that the absolute Bcd concentration is read out during early n.c. 14 (Liu et al., 2013). In comparison data-driven models propose a much wider time window for Bcd readout, as decoding the gradient at its pre-steady-state (Bergmann et al., 2007) or during its degradation (Verd et al., 2017) gives rise to more accurate predictions of gap gene expression patterns. Direct testing of these ideas has previously been difficult due to a lack of temporal manipulation of Bcd activity.

Here we provide the first experimental dissection of the temporal requirements of Bcd transcriptional activity and find unexpected complex temporal patterns of Bcd decoding. Consistent with previous ideas, we find that the time window ranging from n.c. 13 to early n.c. 14 is indeed most critical for Bcd-dependent patterning of downstream genes. Deprivation of Bcd transcriptional activity during this period leads to severe patterning defects in all the Bcd-dependent embryonic regions, from the most anterior to mesothoracic segment (Figures 3F-3G). On the other hand, Bcd activity in this critical time window is sufficient for the proper cell fate induction in mesothorax, regardless of Bcd activity in rest of the time points throughout the blastoderm stage. Further, the more anterior the cells locate, the wider time window of Bcd activity is required (Figure 3), as in the extreme case the proper formation of the most ‘needy’ clypeolabrum segment, patterned by the highest Bcd

362 concentration, requires Bcd-dependent transcription from n.c. 10 to the very end of n.c. 14
363 (Figures 4B-4C).
364
365 Similar correlations between morphogen concentration and required duration have been
366 observed in Shh patterning of the vertebrate neural tube (Dessaud et al., 2007). Shh signalling
367 is temporally integrated by a genetic feedback loop that leads to desensitization of cells to
368 Shh signal over time. In this way, the duration of Shh input is translated into differential gene
369 expression. Considering the rapid establishment Bcd target gene expression patterns, it is
370 unlikely that the same mechanism is utilized here. Our quantitative analysis on gap gene
371 expression stand in line with two alternative mechanisms underlying such temporal
372 integration: (1) The anterior gap genes have slower transcription rates than the posterior gap
373 genes, therefore they require Bcd for longer duration. A recent study has proposed a role of
374 transcription kinetics in shaping the timing as well as the spatial range of morphogen
375 response (Dubrulle et al., 2015). Here, we find that the mRNA production and protein
376 turnover of the anterior gap genes are in a tight balance. Once this balance is tipped by
377 inhibiting transcription even for a short period of time, the protein expression can no longer
378 be maintained (Figure. 6A-6D). In contrast, inhibiting the transcription of more posterior
379 genes, such as hb, in mid to late n.c. 14 does not affect their expression, potentially due to an
380 excessive mRNA pool. (2) Bcd-dependent transcription serves as a priming role in early
381 stages for proper expression of anterior gap genes. Restoring native Bcd dosage in later
382 stages fails to initiate *bona fide* gene expression in the very anterior domains, suggesting that
383 cells are no longer competent to adopt anterior-most cell fates. Whether Bcd primes cell
384 competency by chromosomal remodeling to increase accessibility (Blythe and Wieschaus,
385 2016) or inhibiting the otherwise ectopically expressed repressive factors must be subjected
386 to further investigation.

Temporal interpretation ensures developmental precision by buffering noises

What role does temporal coordination of morphogen interpretation play in achieving precise cell fate determination? In *Drosophila* - as in all long germband insects - the embryonic segments emerge simultaneously (Sander, 1976). Bcd-dependent cell fate specification appears to move from posterior towards the anterior in a sequential manner. The most posterior cells "lock-in" to their correct fate decisions by early cycle 14, becoming refractory to further alterations of Bcd dosage. Meanwhile, more anterior genes remain sensitive to Bcd dosage for much longer periods. Therefore, this mode of temporal interpretation can cope better with a temporally dynamic morphogen gradient or fluctuations in local concentration. This temporal sequence of boundary determination may help to assure robustness of gene boundary specification within such a short developmental time.

Tight coupling between transcription and morphogenesis

Our optogenetic transcriptional manipulation approach brings further insights into how transcription is tightly coupled to cell specification and could be extrapolated to other analyses as morphological movements during embryogenesis. For example, we find that Bcd-dependent transcription not only determines the position of cephalic furrow invagination (Vincent et al., 1997) but also dictates the timing of when this tissue remodeling occurs (Figure S5). Finally, coupling optogenetic manipulations with light-sheet microscopy, we can spatially restrain transcriptional inhibition to one lateral side of the embryo. This locally alters cell fates, resulting in morphological defects – such as in cephalic furrow formation - while the contralateral side remains intact (Movie S2). Spatio-temporal manipulation of Bcd activity in the early embryo is thus an exciting avenue for future study.

Acknowledgments

We thank Eric Wieschaus, Thomas Gregor, Johannes Jaeger, Tiffany Cook, Thomas C. Kaufman and James Sharpe for sharing precious reagents. We acknowledge Eric Wieschaus, Enrique Martin-Blanco, James Briscoe, Philip Ingham, Shelby Blythe and all Saunders' lab members for fruitful discussions. This work was supported by the National Research Foundation Singapore under an NRF Fellowship to T.E.S. (NRF2012NRF-NRFF001-094).

Author Contributions

A.H., C.A. and T.E.S. designed the study. A.H. and C.A. performed the experiments, S.Z. performed the computational analysis and N. S. T. created the Bcd MiMIC mutant. A.H., C.A. and T.E.S. wrote the manuscript. All authors participated in the final version of the manuscript.

The authors declare no competing financial interest.

MATERIALS AND METHODS

Fly stocks and genetics. A CRY2::mCh::Bcd fusion construct was generated by replacing the eGFP sequence in the P[*egfp-bcd*] vector(Gregor et al., 2007a) by the CRY2::mCherry sequence. The original vector was digested with NheI and SphI to remove eGFP and the CRY2::mCherry sequence was amplified by PCR from the AddGene plasmid #26866 (Kennedy et al., 2010) using primers appended with NheI and SphI restriction sites. The resulting **P[*cry2-mcherry-bcd*]** construct contained *bcd* natural 5' and 3' UTRs as well as upstream enhancers. P-element transformation was carried out by BestGene Inc. and seven transgenic lines on the 3rd chromosome were recovered. Two different lines expressing CRY2::mCh::Bcd respectively at low (CRY2^{low}) and high (CRY2^{high}) levels (mCherry fluorescent intensity) were employed throughout our analyses. Transcription and mRNA localization in the transformed flies was expected to recapitulate those of endogenous *bcd*.

A *bcd* knockout fly line was generated by CRISPR-mediated insertion of a MiMIC cassette (Venken et al., 2011) (injection performed by GenetiVision). The progenies from homozygous females phenocopied *bcd*^{E1} developmental defects(Frohnhöfer and Nüsslein-Volhard, 1986). The CRY2::mCh::Bcd (CRY2^{high}) transgenic was recombined with the *bcd* knockout allele to establish a stable line. All experiments were carried out with this fly line unless otherwise stated.

Additionally, the fly line nanos>Gap43::mCh (Martin et al., 2010) was used for light-sheet imaging.

Temporally patterned illumination. Duration of syncytial nuclear cycles were evaluated by imaging embryos on a bright-field stereomicroscope at 25 °C. The blastoderm stage (from fertilization to the onset of gastrulation) spans 2.5 hours. The last syncytial cycle (n.c. 14), demarcated by the last division wave and the first sign of gastrulation, lasts about 45 minutes. The penultimate cycle (n.c. 13) lasts 15 minutes, while the duration of the previous three cycles (n.c. 10-12) is about 30 minutes in total. To maintain dark condition, embryos were observed or imaged with all light sources covered by amber paper (*i.e.* blocking blue light). To induce the conformational change of the CRY2 protein, we illuminated the embryos on a Nikon LED light base at 488 nm wavelength. The light intensity was measured with an intensity power meter. All experiments were carried out at 4.0 mW unless otherwise stated. For temporally patterned illumination, blastoderm stage embryos were selected in the dark condition and exposed to light. The illumination treatment of each embryo was recorded. The illumination duration was timed from the moment of light exposure until the onset of gastrulation. When the illumination treatment was followed by dark recovery, we continued the timing by observing embryos with a light source covered with amber paper until gastrulation initiated.

Immunostaining. Embryos at the desired stages were dechorionated by household bleach and fixed in heptane saturated by 37 % paraformaldehyde (PFA) for 1 hour. The vitelline membrane was subsequently manually removed. Prior to incubation with primary antibodies, embryos were blocked with 10% BSA in PBS. Image-iT®FX signal enhancer was used as blocking reagent instead of 10% BSA for Cad staining. Antibodies used were rabbit anti-mCherry (1:100, AbCam), rat anti-Caudal (1:100), guinea pig anti-Hb (1:2000), rabbit anti-Gt (1:800), guinea pig anti-Kr (1:800), guinea pig anti-Kni (1:800), guinea pig anti-Eve (1:800), guinea pig anti-Otd (1:800), mouse anti En (1:100, DSHB), rabbit anti-Dfd (1:100), mouse anti-Scr (1:10, DSHB), mouse anti-Antp (1:10, DSHB), mouse anti-Ubx (1:100,

DSHB) and mouse anti-Abd-B (1:100, DSHB). Primary antibodies were detected with Alexa Fluor-labelled secondary antibodies (1:500; LifeTech). Embryos were co-stained with Phalloidin conjugated with Alexa Fluor for staging purpose. Embryos were mounted in AquaMount (PolySciences, Inc.) and imaged on a Zeiss LSM710 microscope with a C-Apochromat 40x/1.2 NA water-immersion objective. Cad antibody was kindly provided by Eric Wieschaus. Hb, Gt, Kr, Kni and Eve antibodies were gifts from Johannes Jaeger. Otd was kindly given by Tiffany Cook. Last, Dfd antibody was a gift from Thomas C. Kaufman.

Gradient quantification. Images were projected using a maximum intensity projection and then nuclei segmented using Ilastik (Sommer et al., 2011). Nuclei were binned into 5mm spatial steps along the anterior-posterior axis using Matlab. Bcd nuclear intensity plots were created after background subtraction using morphological opening. Profiles fitted as described in Liu (et al., 2013).

Live imaging and quantification of MS2 RNA reporter. Embryos were collected, dechorionated and mounted on a MatTek dish under dark condition. The embryos were imaged on a custom-built Spinning Disc microscope with a Nikon Apo 40X/1.25 water-immersion objective. The pixel size is 409 nm and the image resolution is 1024x1024 pixels. At each time point a stack of 35 images separated by 3 µm was acquired. The temporal resolution was 40 seconds. Each Z-stack for each time point was Z-projected (maximum intensity) prior to subsequent quantification. The workflow to analyze MS2 spots goes as follow: we extracted the boundary of the embryo to exclude false positive, we applied a threshold and regional intensity comparison to locate all MS2 spots and we tracked these spots using a minimal distance criterion. To refine our analysis, we considered spot tracks lasting for a minimum of 4 time frames. We plotted the probability distribution of MS2 spots persistence into 2 regions, *i.e.* the anterior and posterior domains (Fig. 2e and d). Further, we subdivided the anterior *hb* domain into five distinct regions along the AP axis, *i.e.,* 100-75, 75-70, 70-65, 65-60 and 60-40 %EL. We plotted the probability distribution of MS2 spots persistence in these regions and in the posterior *hb* domain (Extended data Fig 1c and d). MS2 quantification is further described in the Supplementary Materials 1.

Chromatin immunoprecipitation and qPCR. Late n.c. 14 embryos aged in the dark or exposed to light (at 4mW) for 45 minutes were dechorionated in household bleach. Embryos were crosslinked for 15 minutes in a solution containing 2 ml of PBS, 6 ml of Heptane and 180 µl of 20% paraformaldehyde. Embryos were transferred to a 1.5 ml tube and the crosslinking was quenched with the addition of 125 mM glycine in PBS 15 min after the start of fixation. ChIP samples were essentially prepared as described in Blythe and Wieschaus, 2015(Blythe and Wieschaus, 2015). Sonication was performed on a Sartorius stedim Labsonic® M with a microtip horn. An input control corresponding to 2% of the volume per reaction was taken after sonication. Immunoprecipatations (IPs) were performed with a mCherry antibody (Clonetech #632496) for 15 hours at 4ºC. ChIPped DNA were extracted with a Qiaquick spin column (Qiagen). Real-time quantitative PCR was performed using SYBR® Green Assay (Thermo Fisher Scientific) on a Bio-Rad CFX96 Real-time system. Four primer pairs were used, respectively probing Hb (P2 enhancer), Gt, Otd and Kr. Additionality, a primer pair was designed 1kb downstream of the P2 enhancer (HbP2+1kb) to be used as a negative control. The percent input method (100*2^(Adjusted input – Ct(IP)) was used to normalize ChIP-qPCR data. Further, the relative %Input for illuminated embryos was calculated as compared to the embryos in dark and summarized in a bar chart. In the case of the HbP2+1kb, data were compared to HbP2 results. Three independent replicates have been performed for each primer sets and the significance was calculated with a standard t-test.

Cuticle preparation. Embryos subjected to temporally patterned illumination were allowed to develop until the end of embryogenesis. The embryos were then dechorionated and incubated into a mixture of Hoyer's medium and Lactic acid in a 1:1 ratio at 65 °C between an imaging slide and a cover slip. For an exhaustive description of the method used see Alexandre (2008).

Gap gene profile quantification. Confocal Z-stack images were Z-projected (maximum intensity) in Fiji for further analysis. Images were rotated to orient embryos anterior left and dorsal up and rescaled to same embryo length and width. Intensity profiles along the antero-posterior axis were measured in Fiji. For Hb, the intensity profile was normalized to the peak value of the posterior domain. To determine the boundary positions of Kr and Kni expression domains, we plotted the intensity profiles along the AP axis and defined the boundary at the position with intensity equals to half of the peak value.

Hemi embryo illumination on a Light-Sheet microscope. Embryos were dechorionated as described earlier and mounted in 1% agarose on a Fluorinated ethylenepropylene (FEP) capillary (TEF-CAP, #AWG18LW-FEP). Embryos were then imaged on a custom-built Light-Sheet Microscope with a Nikon Apo 1 WD 25X/1.10 water-dipping objective. Embryos expressing CRY2::mCh::Bcd and the membrane marker Gap43::mCh were recorded using a 561nm excitation laser. The pixel size was 510 nm and the image resolution was 1024x1024 pixels. At each time point a stack of 100 images separated by 2.5 µm was acquired. The temporal resolution was 30 seconds. This illumination setup mimics dark condition as no morphological defects were observed. To stimulate CRY2 conformational change in just one half of the embryo, a region on one lateral side of the embryo was defined from the most apical section up to 70 µm down. A stack of 100 sections separated by 0.7 µm were illuminated. The illumination was carried out from the beginning of the n.c. 14 (5 min after the establishment of the cellularization furrow) for 20 min with a 488 nm laser. Following illumination, embryos were imaged solely with the 561 nm excitation laser.

FIGURES

Figure 1

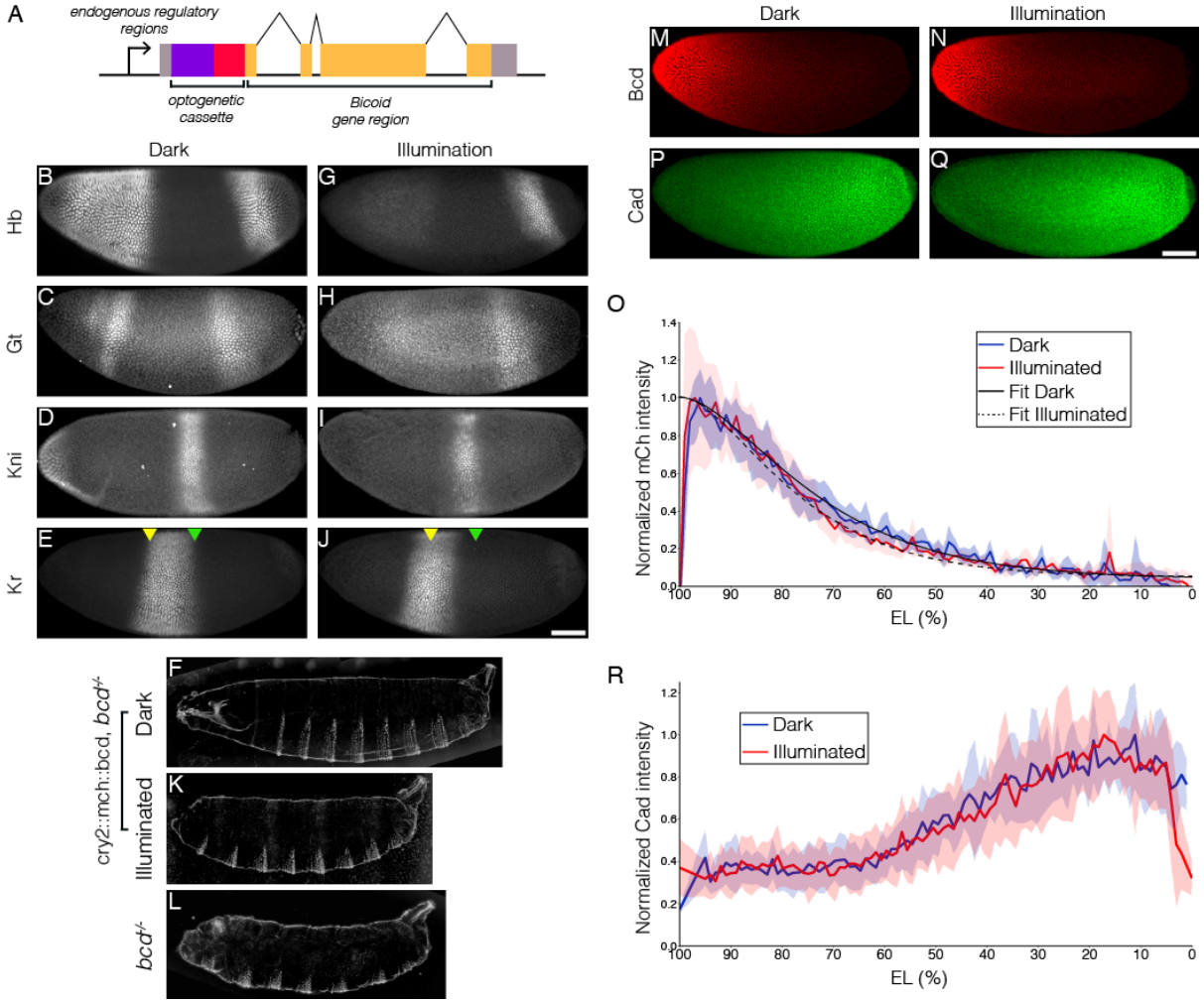

Figure 1. Optogenetic tool to manipulate Bcd-dependent transcription activity

(A) Schematic illustration of CRY2::mCh::Bcd construct; CRY2 optogenetic cassette tagged with mCherry fluorescent protein is fused to the N-terminal of Bcd coding sequence; expression of the construct is under the regulation of the endogenous *bcd* regulatory sequence. (B-J) Embryos having developed in the dark (B-E) or light (G-J) fixed at the end of the blastoderm stage and stained for Hb (B and G), Gt (C and H), Kni (D and I) and Kr (E and J). Yellow and green arrowheads indicate, respectively, the position of the anterior and posterior boundaries in the dark. (F,K and L) Cuticle patterns of embryos with maternally loaded *cry2::mch::bcd* having developed in the dark (F) or light (K) in the first 2.5 h AEL as compared to (L) $bcd^{-/-}$ embryos. (M, N, P and Q) Embryos in the dark (M and P) or light (N and Q) stained for mCh (M and N) and Cad (P and Q) at early n.c. 14.(O and R) Average nuclear intensity of CRY2::mCh::Bcd (O) or Cad (R) normalized to peak value is plotted vs. AP position (% EL) in dark (blue curve) and light (red curve). (O) Data were fitted to an exponential curve shown by smooth lines with length scales around 80 µm. Shaded error bars are across all nuclei of all embryos at a given position. n = 5-7 embryos per condition. Scale bar, 50µm.

Figure 2

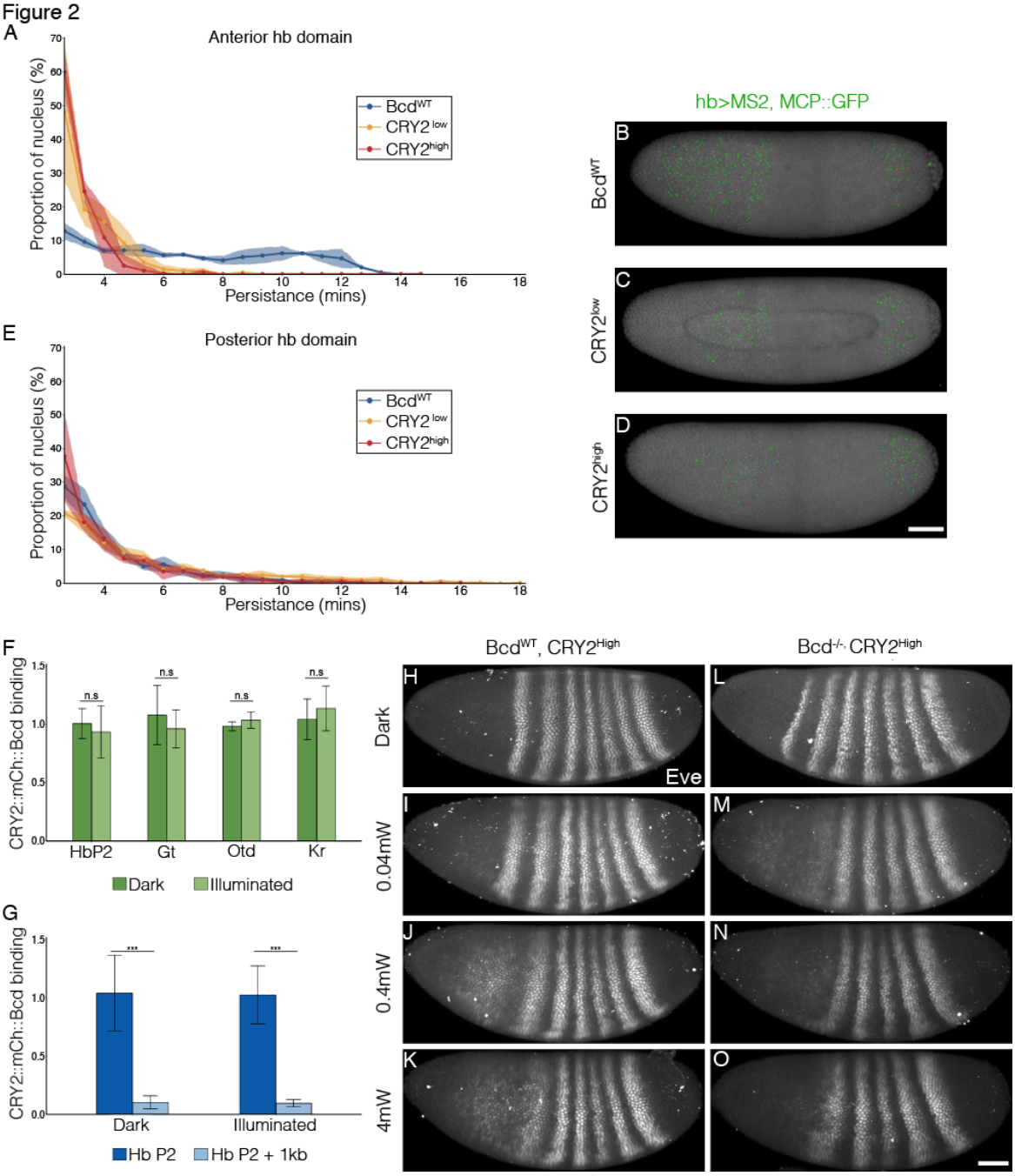

Figure 2. Inhibitory effect on Bcd-dependent transcription is gene-dosage and light-power dependent

(A and E) Proportion of the nuclei positive for *hb* transcription plotted vs. the persistence of transcription activity during n.c. 13 in control (blue), CRY2^{low} (orange) and CRY2^{high} (red) embryos of *hb* anterior (A) and posterior (E) domain. n = 3 embryos per genotype. (B-D) Snapshots of embryos expressing hb>MS2, MCP::GFP in n.c.13. Embryos are maternally loaded with only endogenous *bcd* (B), or together with *cry2::mch::bcd* at low(C) or high (D) level. MCP::GFP signals are tracked and marked with green dots. (F and G) Chromatin immunoprecipitation quantitative PCR (ChIP-qPCR) characterization of CRY2::mCh::Bcd binding to Hb (P2 enhancer), Gt, Otd and Kr in the light for 45 mins (4mW) as compared to embryos aged in the dark (F) and to 1kb downstream of the Hb P2 enhancer in the dark and light conditions (G). (H-O) Eve staining in embryos maternally loaded with cry2::mch::bcd in bcd^{WT} (H-K) or *bcd* null (L-O) background; embryos have developed in dark (H and L) or illuminated with blue light at 0.04mW (I and M), 0.4mW (J and M) or 4mW (K and O). Scale bar, 50µm.

Figure 3

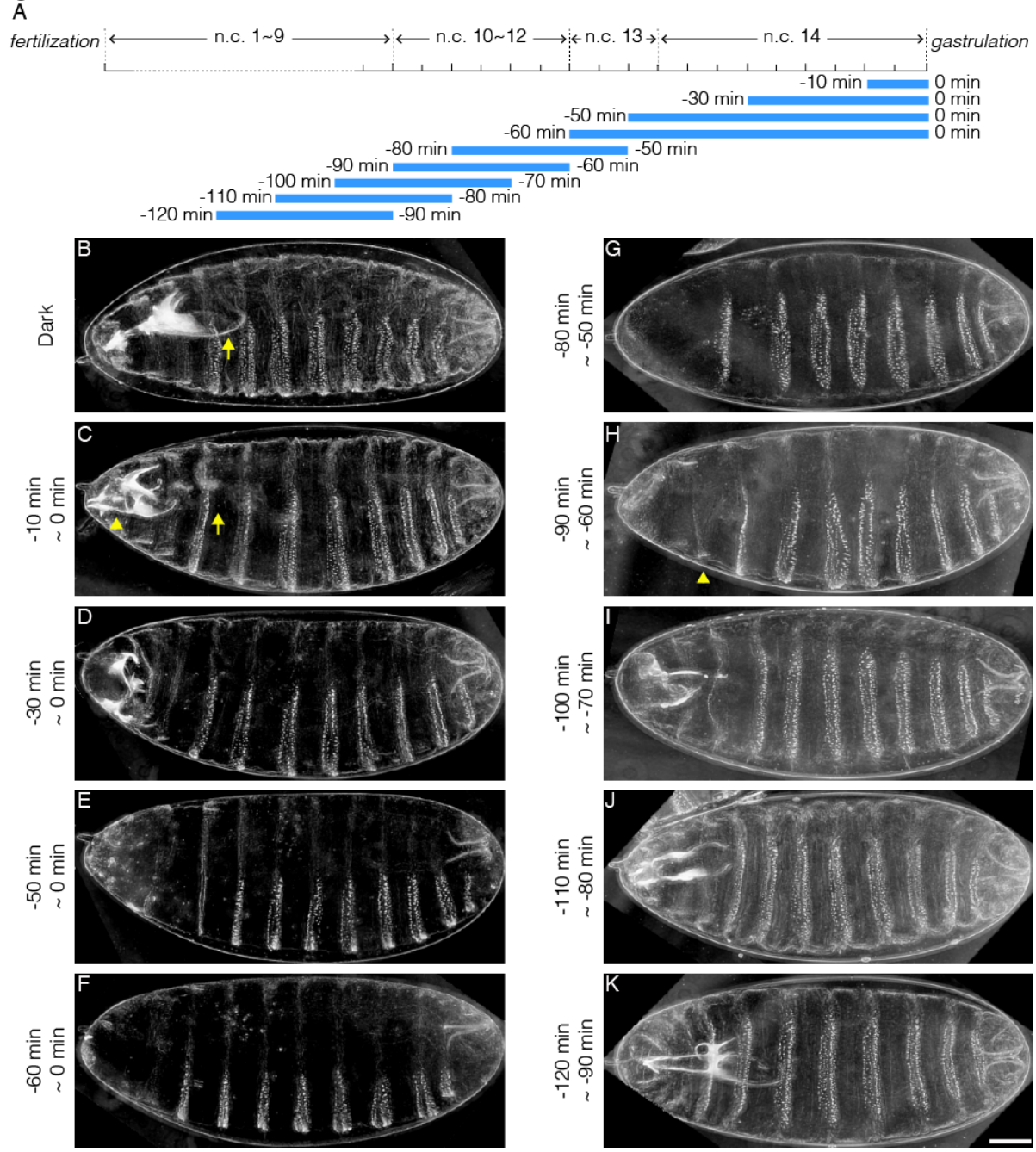

Figure 3. Illumination across different time windows causes embryonic lethality with varied severity

(A) Schematic demonstration of illumination time windows. Blue bars indicate illumination while the absence of blue bars indicates dark condition. The onset of gastrulation is defined as time 0. Negative values refer to specific time before gastrulation. The start and the end of illumination is indicated by the number on the left and right side of the blue bars, respectively. (B-K) Cuticle preparation of embryos illuminated in different time windows. The illumination time is indicated on the left of each image. (B) Arrow, pharynx wall; (C) Arrow, absence of pharynx wall. Arrowhead, missing structures lying between mouth hooks and cephalo-pharyngeal plates. (K) Arrowhead, denticle belt of thorax segment. Scale bar, 50μm.

Figure 4

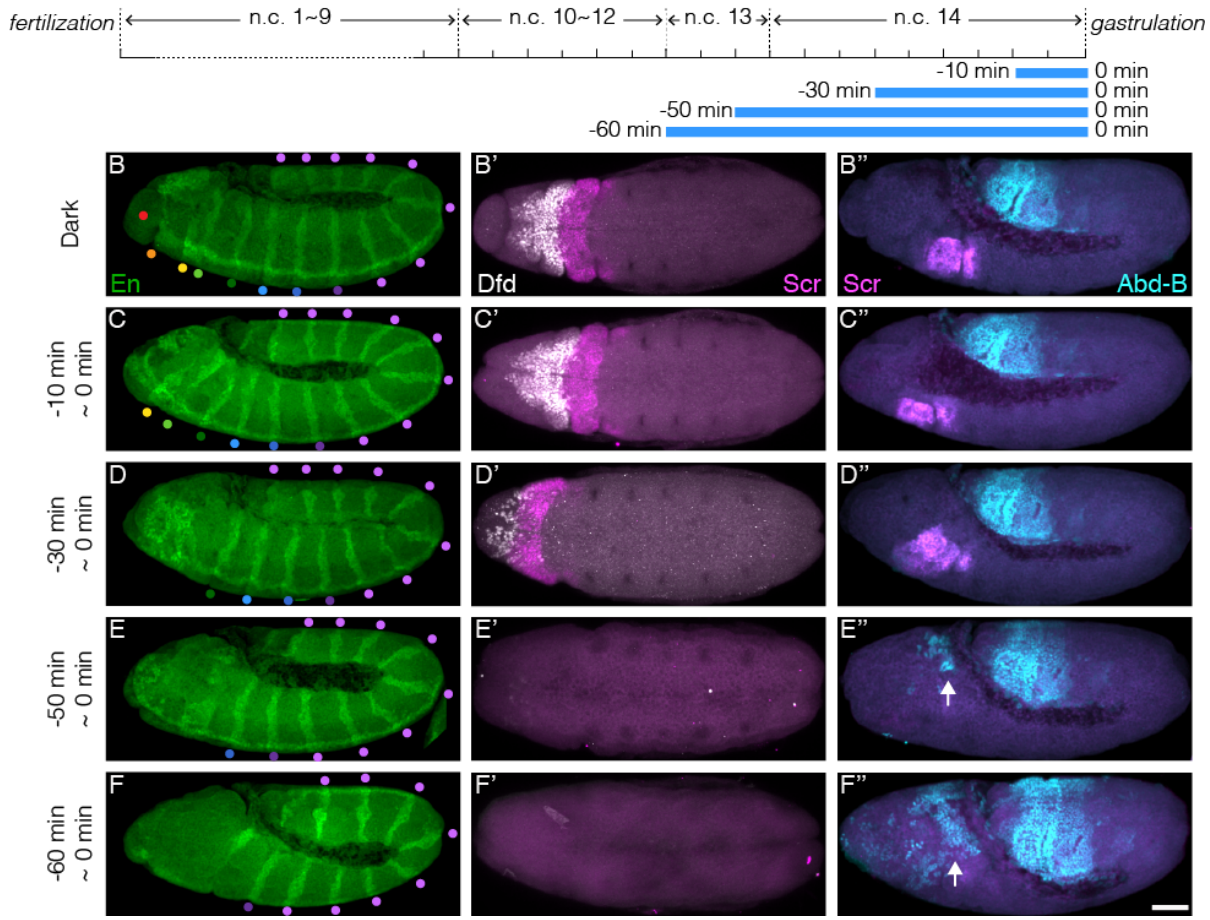

Figure 4. Illumination at the end of blastoderm stage causes wrong cell fate determination in anterior embryonic segments

(A) Schematic demonstration of illumination time windows at the end of blastoderm stage. Illumination starts at certain time before gastrulation and ends at the onset of gastrulation as indicated by blue bars. (B-F, B'-F' and B''-F'') Embryos illuminated in different time windows as indicated at the left side of each panel are fixed by the end of GBE and stained for En (B-F), Deformed (Dfd, white) and Scr (magenta) (B'-F'), Scr (magenta) and Abd-B (cyan)(B''-F''); (B-F) Colored dots represent embryonic segments. Red, clypeolabrum; orange, stomodeum; yellow, mandibular lobe; light green, maxillary lobe; dark green, labial lobe; light blue, prothorax; dark blue, mesothorax; dark purple, metathorax; and light purple, abdominal segments. (E'' and F'') Arrows, ectopic Abd-B expression. Scale bar, 50μm.

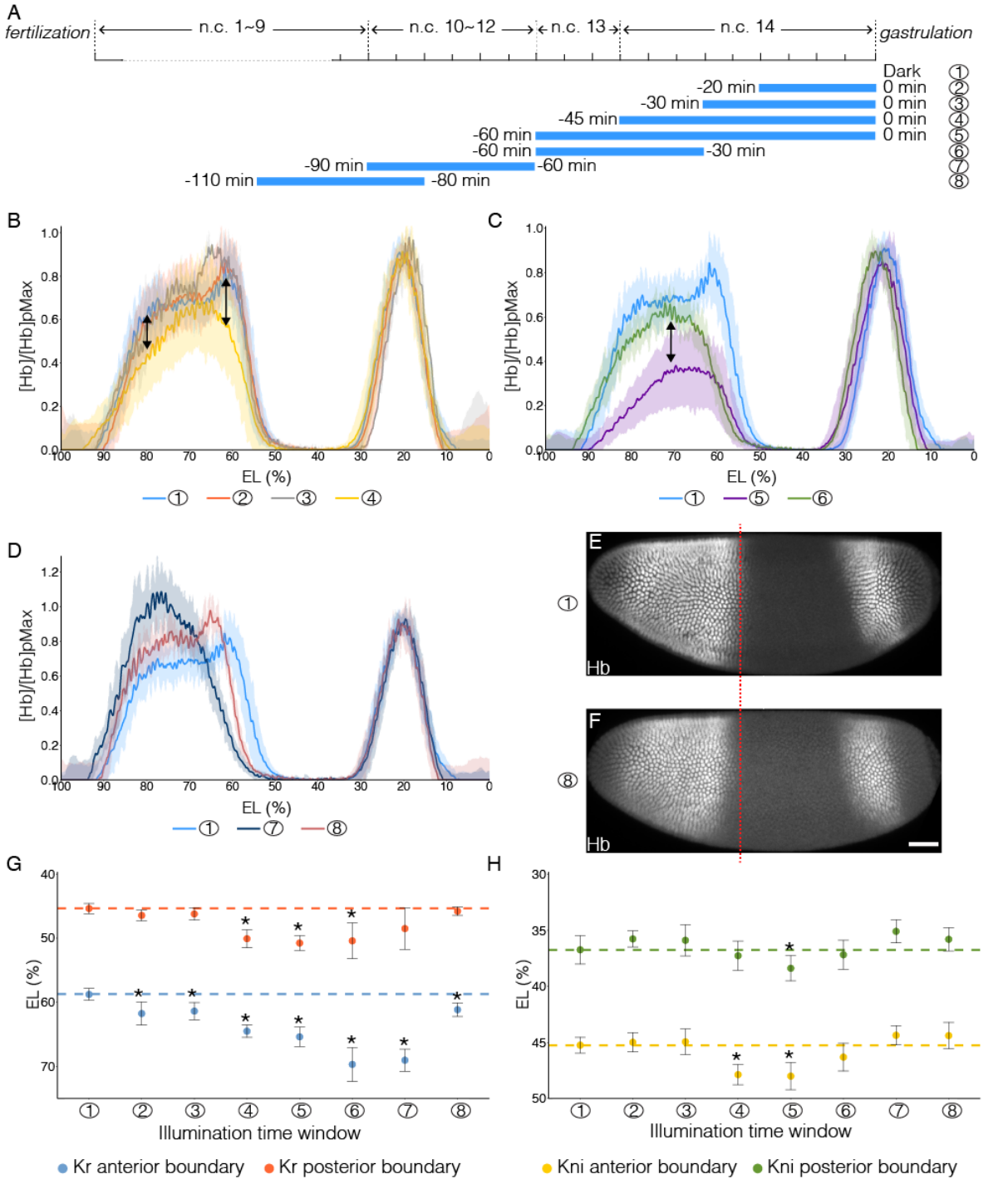

Figure 5. Impact of temporally patterned illumination on downstream gene expression

(A) Schematic demonstration of eight different illumination time windows. (B-D) Average Hb intensity normalized to posterior peak values plotted vs. AP position (% EL) in embryos having developed in different temporally patterned illumination. Sample numbers correspond to time windows shown in (A). (B-C) Double-headed arrows point out the changed expression level of Hb. (E and F) Embryos having developed in dark (E) or illuminated for 30 minutes before n.c.11 (F) are stained for Hb. Red dashed line indicates the position of posterior border of anterior Hb domain of embryo in (e). Scale bar, 50µm. (G and H) Position of Kr anterior border (G, blue dots), Kr posterior border (G, red dots), Kni anterior border (H, yellow dots) and Kni posterior border (H, green dots) under different temporal illumination as indicated by sample numbers. Error bars indicate s.d.; t-test was used for the statistical evaluation with *p<0.05. A total number of 70, 53 and 59 embryos were analyzed for expression of Hb, Kr and Kni, respectively.

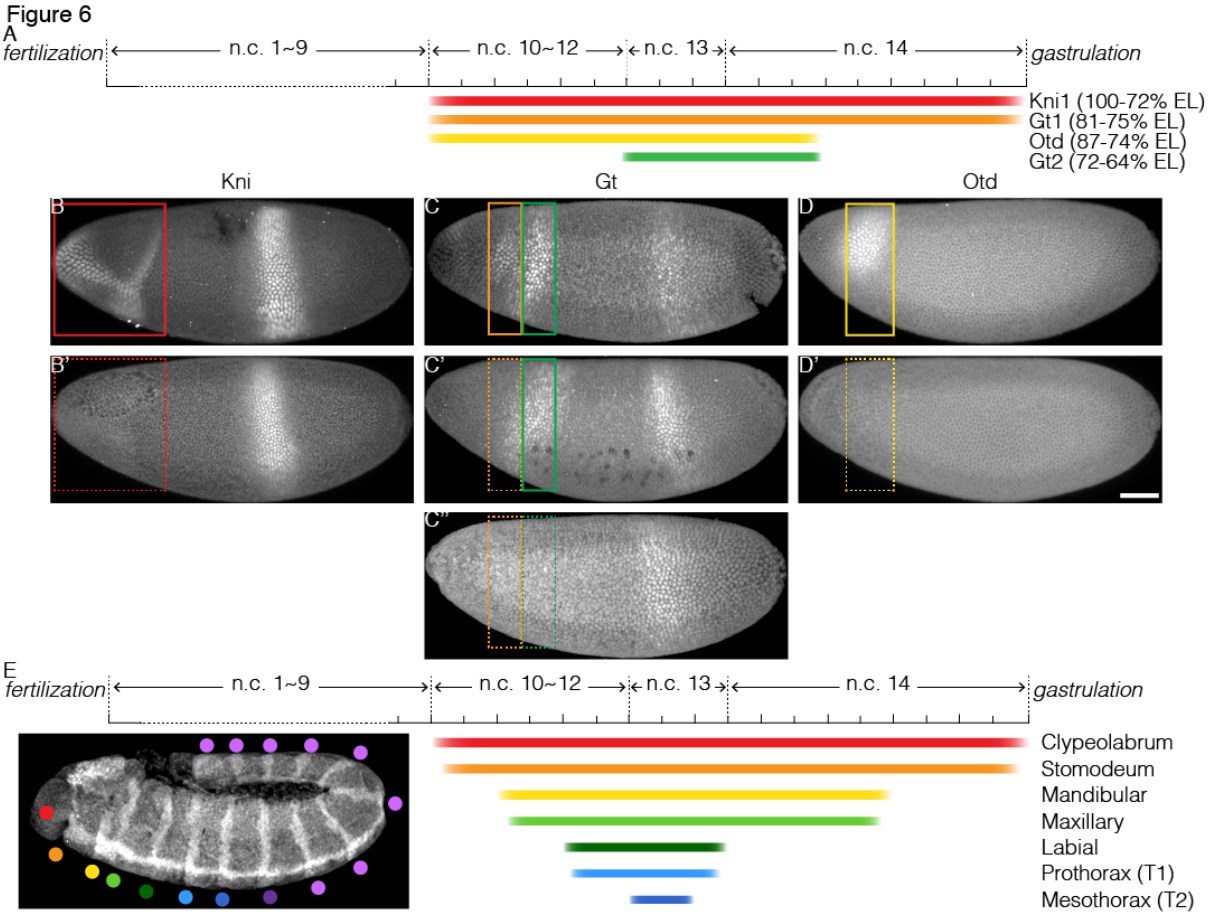

Figure 6. Temporal requirement of Bcd-dependent transcription for proper cell fate determination

(A) Schematic representation of required time windows of Bcd-dependent transcription for downstream gene expression; color bars indicate the time windows required for Bcd-dependent transcription to be on for correct expression of Kni1 (red), Gt1 (orange), Otd (yellow) and Gt2 (green); (B-D) embryos exhibiting the correct gene expression when Bcd-dependent transcription is active in required time window; colored boxes point out the corresponding expression domain; (B'-D' and C'') embryos showing defects in gene expression when Bcd-dependent transcription is interrupted in required time window; dashed boxes indicate failed expression. Scale bar 50μm. (E) Schematic diagram of temporal interpretation of Bcd morphogen. Colored bars indicate the time windows required for Bcd-dependent transcription for correct cell fate determination in different embryonic segments.

Figure S1

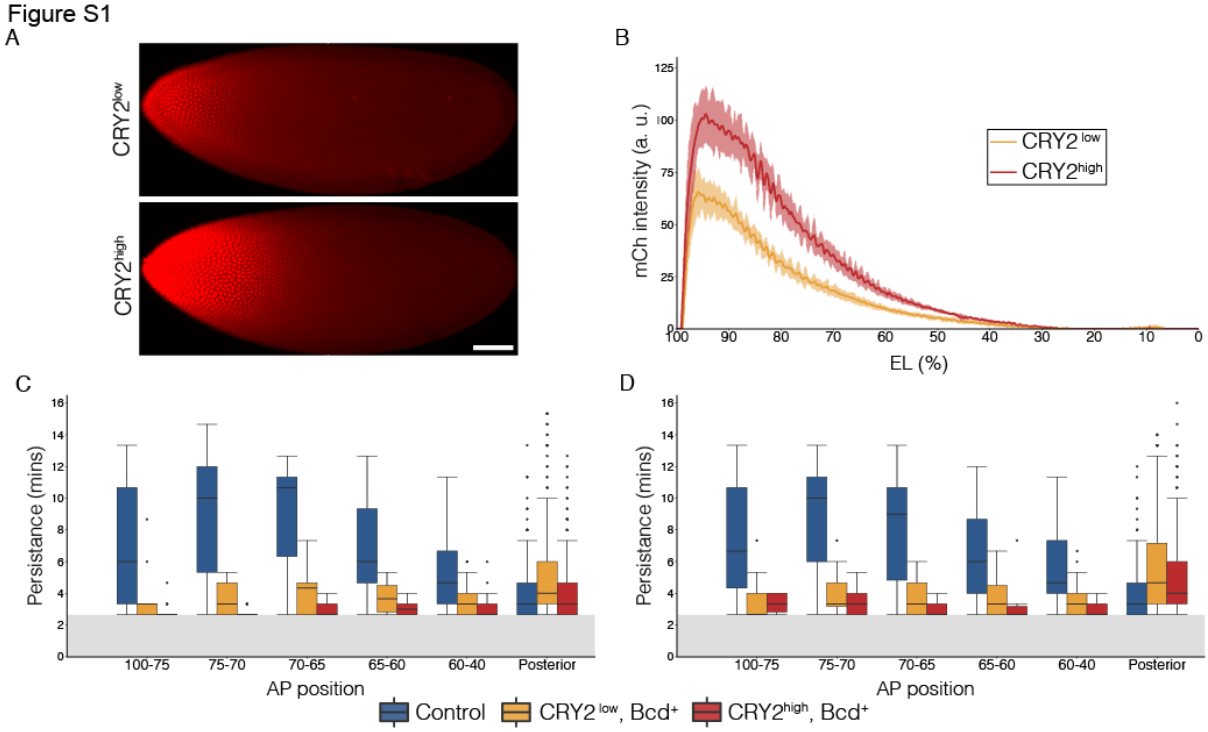

Figure S1. Expression profiles in CRY2^{low} and CRY2^{high} embryos and effect of illumination on hb mRNA production along the AP axis

(A) Snapshots of embryos expressing CRY2::mCh::Bcd at comparatively low (top panel) and high (bottom panel) level at late n.c. 14. Scale bar, 50 µm. (B) Average nuclear mCherry intensity in CRY2^{low} (orange curve) and CRY2^{high} (red curve) embryos at late n.c. 14 is plotted vs AP position (% EL). Shaded error bars are across all nuclei of all embryos at a given position. n = 8 embryos for CRY2^{low} and n = 5 embryos for CRY2^{high}. (C and D) Box plot showing the persistence of *hb*>MS2 puncta in control (blue), CRY2^{low} (orange) and CRY2^{high} (red) embryos. Anterior *hb* domain is subdivided into five distinct regions along AP axis, *i.e.,* 100-75, 75-70, 70-65, 65-60 and 60-40% EL. Data is quantified in these regions as well as *hb* posterior domain, respectively. The cutoff value for statistical analysis is 160s as shown by the grayed regions. Each box shows the counts for a single embryo.

Figure S2

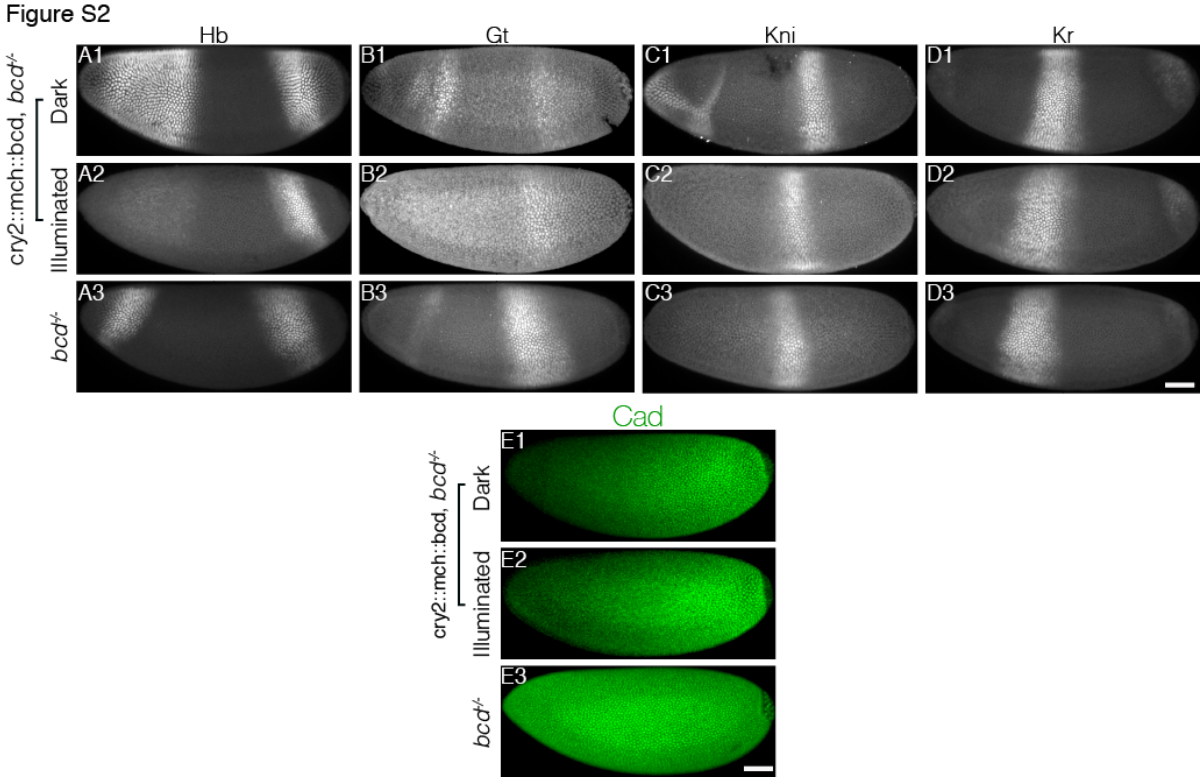

Figure S2. Comparison of gap gene and Caudal expression patterns between optogenetic and *bcd* mutant embryos

(A-E) Embryos laid by females expressing CRY2::mCh::Bcd in a *bcd* null background having developed in the dark (A1-E1) or light (A2-E2), or by females of *bcd* mutant (A3-E3) fixed at the end of blastoderm stage and stained for Hb (A1-A3), Gt (B1-B3), Kr (C1-C3) and Kni (D1-D3), or fixed at early n.c.14 and stained for Cad (E1-E3). Scale bar, 50 µm.

Figure S3

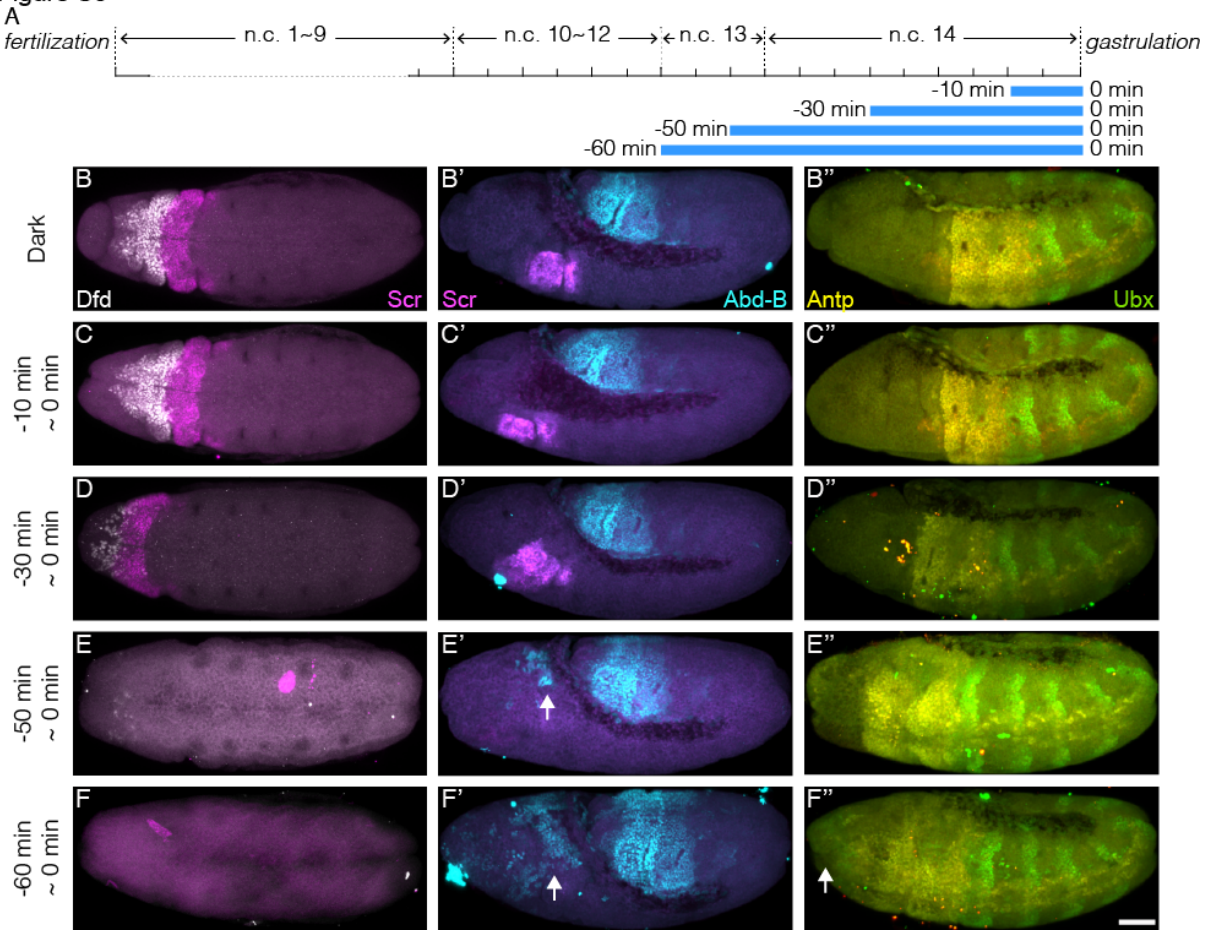

Figure S3. Hox genes expression pattern in increasing illumination time window

(A) Schematic demonstration of illumination time windows at the end of blastoderm stage. Illumination starts at certain time before gastrulation and ends at the onset of gastrulation as indicated by blue bars. (B-F, B'-F' and B''-F'') Embryos illuminated in different time windows as indicated on the left side of each panel are fixed by the end of GBE and stained for Dfd (white) and Scr (magenta) (B-F), Scr (magenta) and Abd-B (B'-F') and Antp (yellow) and Ubx (green)(B''-F''). Panels (B-F) and (B'-F') show the unprocessed images previously shown in Figure 4. (E' and F') Arrows, ectopic Abd-B expression. (F'') Arrow, ectopic Ubx expression. Scale bar, 50 μm.

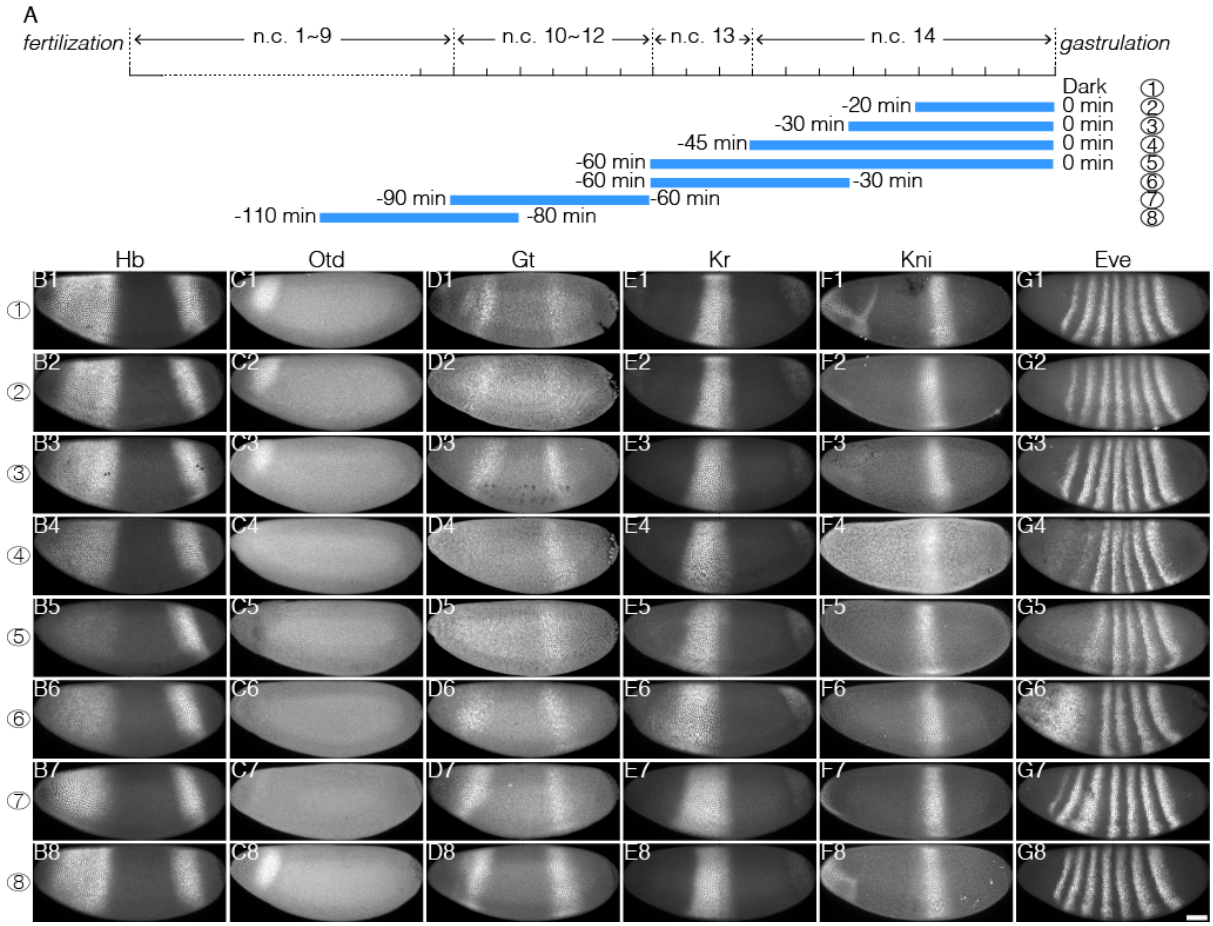

Figure S4. Impact of temporally patterned illumination on downstream gene expression
(A) Schematic demonstration of eight different illumination time windows. (B-G) Embryos illuminated in different time windows are fixed at the end of blastoderm stage and stained for Hb (B1-B8), Otd (C1-C8), Gt (D1-D8), Kr (E1-E8), Kni (F1-F8), and Eve (G1-G8); row 1-8 corresponds to 8 temporal illumination conditions shown in (A). Scale bar, 50 μm.

Figure S5

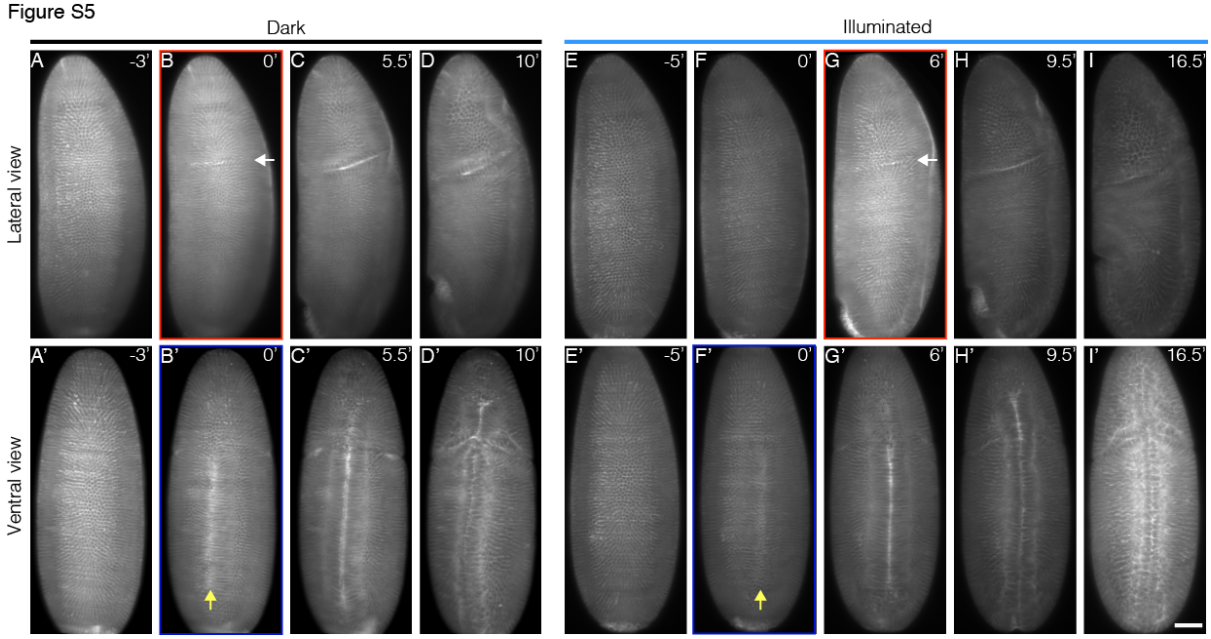

Figure S5. Impeding Bcd-dependent transcription during cycle 14 delays cephalic furrow invagination

Embryos expressing CRY2::mCh::Bcd and Gap43::mCh are imaged on a custom built light-sheet microscope. The embryos are illuminated with a 488nm laser for 20min starting 5min after the establishment of the cellularization furrow. Panels (A-D) and (A'-D') show respectively the lateral and ventral views for dark control embryos while (E-I) and (E'-I') show the lateral and ventral views for illuminated embryos. The red and blue rectangles indicate the time point marking the onset of cephalic furrow (white arrows) and ventral furrow (yellow arrows) invagination, respectively. Scale bar, 50 μm.

Movie S1. CRY2::mCh::Bcd expression reduces the transcription activity of hb in the anterior domain in blue light

Embryos expressing the hb>MS2, MCP::GFP system were imaged throughout n.c. 13 and 14 with a time resolution of 40s. Rows 1, 2 and 3 show respectively Control, $CRY2^{low}$ and $CRY2^{high}$ embryos. The left column represents the raw data whilst the right column shows the segmented MS2 dots (in green) as described in the Methods section.

Movie S2. Bilateral cephalic furrow formation is uncoupled by single sided illumination

Embryo expressing CRY2::mCh::Bcd and Gap43::mCh mounted on a custom-built Light-Sheet microscope. The embryo was mounted during n.c. 13 and Gap43::mCh was used to follow its developmental stage. Five minutes after the start of cellularization, one lateral side of the embryo was illuminated for 20min, starting from its most apical section to 70µm deep (0.7µm interval). Whole embryo recording (561nm laser) and hemi embryo illumination (488nm laser) were done simultaneously with a time resolution of 30s. The top two panels show the lateral sides of the embryo, the second panel being the illuminated one. The bottom two panels show the ventral and the dorsal, respectively.

693 **REFERENCES**

694 Alexandre, C. (2008). Cuticle Preparation of Drosophila Embryos and Larvae. Methods Mol.
695 Biol. 197–205.

696 Ali-Murthy, Z., and Kornberg, T.B. (2016). Bicoid gradient formation and function in the
697 Drosophila pre-syncytial blastoderm. Elife *5*, 1–18.

698 Bergmann, S., Sandler, O., Sberro, H., Shnider, S., Schejter, E., Shilo, B.Z., and Barkai, N.
699 (2007). Pre-steady-state decoding of the bicoid morphogen gradient. PLoS Biol. *5*, 0232–
700 0242.

701 Blythe, S.A., and Wieschaus, E.F. (2015). Zygotic genome activation triggers the DNA
702 replication checkpoint at the midblastula transition. Cell *160*, 1169–1181.

703 Blythe, S.A., and Wieschaus, E.F. (2016). Establishment and maintenance of heritable
704 chromatin structure during early *Drosophila* embryogenesis. Elife *5*, e20148.

705 Dessaud, E., Yang, L.L., Hill, K., Cox, B., Ulloa, F., Ribeiro, A., Mynett, A., Novitch, B.G.,
706 and Briscoe, J. (2007). Interpretation of the sonic hedgehog morphogen gradient by a
707 temporal adaptation mechanism. Nature *450*, 717–720.

708 Dessaud, E., Ribes, V., Balaskas, N., Yang, L.L., Pierani, A., Kicheva, A., Novitch, B.G.,
709 Briscoe, J., and Sasai, N. (2010). Dynamic assignment and maintenance of positional identity
710 in the ventral neural tube by the morphogen sonic hedgehog. PLoS Biol. *8*.

711 Driever, W., Thoma, G., and Nusslein-Volhard, C. (1989). Determination of spatial domains
712 of zygotic gene expression in the Drosophila embryo by the affinity of binding sites for the
713 bicoid morphogen. Nature *340*, 363–367.

714 Dubrulle, J., Jordan, B.M., Akhmetova, L., Farrell, J.A., Kim, S.H., Solnica-Krezel, L., and
715 Schier, A.F. (2015). Response to Nodal morphogen gradient is determined by the kinetics of
716 target gene induction. Elife *4*, 1–27.

717 Frasch, M., and Levine, M. (1987). Complementary patterns of even-skipped and fushi tarazu
718 expression involve their differential regulation by a common set of segmentation genes in
719 Drosophila. Genes Dev. *1*, 981–995.

720 Frohnhöfer, H.G., and Nüsslein-Volhard, C. (1986). Organization of anterior pattern in the
721 Drosophila embryo by the maternal gene bicoid. Nature *324*, 120–125.

722 Garcia, H.G., Tikhonov, M., Lin, A., and Gregor, T. (2013). Quantitative imaging of
723 transcription in living Drosophila embryos links polymerase activity to patterning. Curr. Biol.
724 *23*, 2140–2145.

725 Gregor, T., Tank, D.W., Wieschaus, E.F., and Bialek, W. (2007a). Probing the Limits to
726 Positional Information. Cell *130*, 153–164.

727 Gregor, T., Wieschaus, E.F., McGregor, A.P., Bialek, W., and Tank, D.W. (2007b). Stability
728 and Nuclear Dynamics of the Bicoid Morphogen Gradient. Cell *130*, 141–152.

729 Guglielmi, G., Barry, J.D., Huber, W., and De Renzis, S. (2015). An Optogenetic Method to
730 Modulate Cell Contractility during Tissue Morphogenesis. Dev. Cell.

731 Gurdon, J.B., and Bourillot, P.Y. (2001). Morphogen gradient interpretation. Nature *413*,
732 797–803.

733 Harfe, B.D., Scherz, P.J., Nissim, S., Tian, H., McMahon, A.P., and Tabin, C.J. (2004).
734 Evidence for an expansion-based temporal Shh gradient in specifying vertebrate digit
735 identities. Cell *118*, 517–528.

Hoch, M., Seifert, E., and Jäckle, H. (1991). Gene expression mediated by cis-acting sequences of the Krüppel gene in response to the Drosophila morphogens bicoid and hunchback. EMBO J. *10*, 2267–2278.

Hülskamp, M., Pfeifle, C., and Tautz, D. (1990). A morphogenetic gradient of hunchback protein organizes the expression of the gap genes Krüppel and knirps in the early Drosophila embryo. Nature *346*, 577–580.

Jaeger, J., Surkova, S., Blagov, M., Janssens, H., Kosman, D., Kozlov, K.N., Manu, Myasnikova, E., Vanario-Alonso, C.E., Samsonova, M., et al. (2004). Dynamic control of positional information in the early Drosophila embryo. Nature *430*, 368–371.

Johnson, H.E., Goyal, Y., Pannucci, N.L., Schüpbach, T., Shvartsman, S.Y., and Toettcher, J.E. (2017). The Spatiotemporal Limits of Developmental Erk Signaling. Dev. Cell *40*, 185–192.

Kennedy, M.J., Hughes, R.M., Peteya, L. a, Schwartz, J.W., Ehlers, M.D., and Tucker, C.L. (2010). Rapid blue-light-mediated induction of protein interactions in living cells. Nat. Methods *7*, 973–975.

Kraut, R., and Levine, M. (1991). Spatial regulation of the gap gene giant during Drosophila development. *609*.

Little, S.C., Tkačik, G., Kneeland, T.B., Wieschaus, E.F., and Gregor, T. (2011). The formation of the bicoid morphogen gradient requires protein movement from anteriorly localized mRNA. PLoS Biol. *9*.

Liu, F., Morrison, A.H., and Gregor, T. (2013). Dynamic interpretation of maternal inputs by the Drosophila segmentation gene network. Proc. Natl. Acad. Sci. U. S. A. *110*, 6724–6729.

Lucas, T., Ferraro, T., Roelens, B., De Las Heras Chanes, J., Walczak, A.M., Coppey, M., and Dostatni, N. (2013). Live Imaging of Bicoid-Dependent Transcription in Drosophila Embryos. Curr. Biol. *23*, 2135–2139.

Lucchetta, E.M., Lee, J.H., Fu, L.A., Patel, N.H., and Ismagilov, R.F. (2005). Dynamics of Drosophila embryonic patterning network perturbed in space and time using microfluidics. Nature *434*, 1134–1138.

Manu, Surkova, S., Spirov, A., Gursky, V., Janssens, H., Kim, A.-R., Radulescu, O., Vanario-Alonso, C.E., Sharp, D.H., Samsonova, M., et al. (2009). Canalization of Gene Expression in the Drosophila Blastoderm by Gap Gene Cross Regulation. PLoS Biol. *7*, e1000049.

Martin, A.C., Gelbart, M., Fernandez-Gonzalez, R., Kaschube, M., and Wieschaus, E.F. (2010). Integration of contractile forces during tissue invagination. J. Cell Biol. *188*, 735–749.

Neumann, C., and Cohen, S. (1997). Morphogens and pattern formation. Bioessays *19*, 721–729.

Perry, M.W., Boettiger, A.N., and Levine, M. (2011). Multiple enhancers ensure precision of gap gene-expression patterns in the Drosophila embryo. Pnas *108*, 1–12.

Perry, M.W., Bothma, J.P., Luu, R.D., and Levine, M. (2012). Precision of hunchback expression in the Drosophila embryo. Curr. Biol. *22*, 2247–2252.

Sako, K., Pradhan, S.J., Barone, V., Inglés-Prieto, Á., Müller, P., Ruprecht, V., Čapek, D., Galande, S., Janovjak, H., and Heisenberg, C.-P. (2016). Optogenetic Control of Nodal Signaling Reveals a Temporal Pattern of Nodal Signaling Regulating Cell Fate Specification during Gastrulation. Cell Rep. 866–877.

780 Sander, K. (1976). Specification of the Basic Body Pattern in Insect Embryogenesis. Adv. In
781 Insect Phys. *12*, 125–238.

782 Sommer, C., Straehle, C., Ullrich, K., and Hamprecht, F. a (2011). Ilastik: Interactive
783 learning and segmentation toolkit. Eighth IEEE Int. Symp. Biomed. Imaging 230–233.

784 Stanojevic, D., Small, S., and Levine, M. (2016). Regulation of a Segmentation Stripe by
785 Overlapping Activators and Repressors in the Drosophila Embryo. *254*, 1385–1387.

786 Struhl, G., Struhl, K., and Macdonald, P.M. (1989). The gradient morphogen bicoid is a
787 concentration-dependent transcriptional activator. Cell *57*, 1259–1273.

788 Tucker, J.A., Mintzer, K.A., and Mullins, M.C. (2008). The BMP Signaling Gradient Patterns
789 Dorsoventral Tissues in a Temporally Progressive Manner along the Anteroposterior Axis.
790 Dev. Cell *14*, 108–119.

791 Turing, A.M. (1990). The chemical basis of morphogenesis. Bull. Math. Biol. *52*, 153–197.

792 Venken, K.J.T., Schulze, K.L., Haelterman, N. a, Pan, H., He, Y., Evans-Holm, M., Carlson,
793 J.W., Levis, R.W., Spradling, A.C., Hoskins, R. a, et al. (2011). MiMIC: a highly versatile
794 transposon insertion resource for engineering Drosophila melanogaster genes. Nat. Methods
795 *8*, 737–743.

796 Verd, B., Crombach, A., and Jaeger, J. (2017). Dynamic Maternal Gradients Control Timing
797 and Shift-Rates for Drosophila Gap Gene Expression. PLoS Comput. Biol. *13*, e1005285.

798 Vincent, A., Blankenship, J.T., and Wieschaus, E. (1997). Integration of the head and trunk
799 segmentation systems controls cephalic furrow formation in Drosophila. Development *124*,
800 3747–3754.

801 Wolpert, L. (1969). Positional information and the spatial pattern of cellular differentiation. J.
802 Theor. Biol. *25*, 1–47.